DOI: 10.1021/ma9012576

Macromolecules
ARTICLE

Precipitated Calcium Carbonate Hybrid Hydrogels: Structural and Mechanical Properties

Murat Guvendiren,[†] Paul A. Heiney,[‡] and Shu Yang*,[†]

[†]*Department of Materials Science and Engineering, 3231 Walnut Street, University of Pennsylvania, Philadelphia, Pennsylvania 19104, and* [‡]*Department of Physics and Astronomy, 209 South 33rd Street, University of Pennsylvania, Philadelphia, Pennsylvania 19104*

Received June 11, 2009; Revised Manuscript Received July 16, 2009

ABSTRACT: Hybrid hydrogels consisting of 2-hydroxyethyl methacrylate (HEMA), methyl methacrylate (MMA) prepolymers, and precipitated calcium carbonate (PCC) were prepared through a two-stage photo-cross-linking process. To elucidate the effects of PCC morphology, size, aspect ratio, and concentration to the structural and mechanical properties of the hybrid hydrogels, two types of PCC, including rhombohedral calcite with particle size of 50−150 nm and needle-shape aragonite with particle size of 380−1250 nm and aspect ratio of 4.2−6.6, were investigated. In all cases, the PCCs were found randomly dispersed in the hydrogel network. A significant increase in both shear and Young's moduli was observed in hybrid gels with larger PCC particle size and aspect ratio 40−180 MPa from aragonite and 20−150 MPa from calcite compared to 3 MPa in the neat hydrogels (60/40 wt % HEMA/MMA). Consistent with modulus data, the network mobility decreased with increasing particle concentration, particle size, and aspect ratio, and the hybrid gels from calcite PCC showed more efficient stress relaxation in comparison to that from aragonite PCC particles.

Introduction

Hydrogels are functional soft materials which can absorb a large quantity of water while maintaining their three-dimensional open network structures. They are particularly attractive for biological applications, including drug delivery, tissue engineering, bioadhesives, biosealants, and biosensors.[1−4] However, in the swollen state, traditional hydrogel networks are highly stretched, therefore, exhibiting poor mechanical properties and limited functionalities. Recently a number of strategies have been studied to produce mechanically strong hydrogels with enhanced functionality, including double network (DN) gels,[5−8] interpenetrating network (IPN) gels,[3,9−11] semi-interpenetrating network (s-IPN) gels,[12,13] natural polymer gels,[14−16] and nanocomposite (NC) or hybrid gels.[17−19] Among them, the incorporation of inorganic fillers in hydrogels is intriguing. By varying the type, size, and morphology of the fillers and their loading, the hybrid gels can possess superior mechanical, optical, electrical, and thermal conductivity and stimuli responsiveness. The fillers in these systems can be integrated into the network framework through covalent or hydrogen bonding or simply by physical mixing to support the network structure. For example, hydrogel nanocomposites prepared by free-radical polymerization in the presence of clay showed enhanced mechanical strength with tunable swelling ratio, optical transparency, and thermal sensitivity.[17,19−22] When mixed with Au and Ag nanoparticles and graphite, electrical and thermal conductivity of hydrogel nanocomposites are increased.[23,24] In the case of polymer nanocomposites with carbon nanotubes (CNTs), it has been shown that the aspect ratio, concentration, and axial orientation of the CNTs play important roles in CNT percolation threshold and electrical, thermal, and mechanical properties of the composites.[25−27] In general, the properties of the composites are highly dependent on the chemical and physical nature of the fillers, including size and size distribution, morphology, aspect ratio, surface chemistry, hardness, conductivity, and refractive index.[26] Among a wide range of studied polymer composites, the effects of filler morphology, size, and aspect ratio on mechanical properties of hydrogel composites remains less understood. Here, using a model hydrogel system consisting of water-soluble 2-hydroxyethyl methacrylate (HEMA) and glassy hydrophobic methyl methacrylate (MMA) polymers, ethylene glycol dimethacrylate (EGDMA) as the cross-linker, and precipitated calcium carbonate (PCC) particles as fillers, we investigated the structural and mechanical properties of the hybrid hydrogels.

As one of the most abundant biominerals, calcium carbonate ($CaCO_3$) has attracted much interest as inorganic additives. $CaCO_3$ exists a variety of polymorphs, of which there are three anhydrous crystalline polymorphs, calcite, aragonite, and vaterite.[28] Calcite is the most stable and abundant polymorph with rhombohedral, orthorhombic, and hexagonal morphologies, aragonite is somewhat less stable with needle-shape orthorhombic crystal structure, and vaterite is metastable. PCC particles are refined, synthetic $CaCO_3$. They are commercially available with different morphologies, uniform particle size ranging from nano- to macroscale, and high purity (>96%), which makes them attractive as low-cost functional additives. For example, both calcite and aragonite PCCs have been widely used in paper, pharmaceutical, packaging, coatings, and food industries.[28−32]

In our system, the hybrid hydrogels were prepared by dispersing PCC particles in a partially polymerized, viscous liquid of poly(2-hydroxyethyl methacrylate-*co*-methyl methacrylate) (PHEMA-*co*-PMMA), followed by photo-cross-linking with EGDMA. We optimized the swelling and mechanical properties of the hydrogels by varying the relative composition of the hydrophobic, glassy component (MMA) in PHEMA-*co*-PMMA random copolymers. To investigate the effects of filler morphology, size, and aspect ratio, we used two types of PCCs, including

*Corresponding author. E-mail: shuyang@seas.upenn.edu.

 Published on Web 07/23/2009

rhombohedral calcite with particle size of 50−150 nm and an aspect ratio of 1 and needle-shape aragonite PCC with particle size of 380 and 1250 nm and an aspect ratio of 4.2−6.6. The filler volume fraction was varied between 0.02 and 0.20 (or 0.05−0.4 weight fraction). Fourier transform infrared (FT-IR) spectroscopy and wide-angle X-ray scattering (WAXS) studies suggested that PCC were physically mixed into the gel network, and such mixing was random as further confirmed by small-angle X-ray scattering (SAXS) and SEM images. The equilibrium water weight fraction of the hybrid gels decreased modestly to 0.1−0.15 from the neat hydrogels (0.17 ± 0.02), which was found, however, independent of PCC particle size and morphology. Shear rheology and compression tests on hybrid gels showed a significant increase in mechanical properties, and the magnitude was dependent on the particle size, morphology, aspect ratio, and concentration. Overall, the modulus values were higher from aragonite/hydrogels than that of calcite/hydrogels: the compressive moduli of the hybrid hydrogels were 40−180 MPa from aragonite and 20−150 MPa from calcite. Stress relaxation experiments showed that the calcite hybrid hydrogels relaxed more efficiently than the aragonite hybrids.

Experimental Section

Materials. Methyl methacrylate (MMA, Aldrich), 2-hydroxyethyl methacrylate (HEMA, Acros Organics), ethylene glycol dimethacrylate (EGDMA, Alfa Aesar), and 2-hydroxy-2-methyl-1-phenylpropan-1-one, under trade name Darocur 1173 (Ciba Specialty Chemicals Inc.), were used as received. Precipitated calcium carbonate ($CaCO_3$) (PCC) particles in calcite (rhombohedral) and aragonite (orthorhombic, needle shape) crystal forms were obtained from Specialty Minerals and Mississippi Lime, respectively (see Table S1 in the Supporting Information).

Hydrogel Synthesis. PHEMA-*co*-PMMA hydrogels with various HEMA to MMA ratios (see Table S2 in the Supporting Information) were photo-cross-linked from viscous, partially polymerized PHEMA-*co*-PMMA prepolymers with EGDMA.[33] In a typical procedure, 2 mL of HEMA/MMA monomer solution was mixed with 60 μL of Darocur 1173 (photoinitiator) in a 20 mL glass vial and exposed to UV light (model B100 AP, UVP Black Ray, ~8 mW/cm^2) for a desired amount of time. The precursor solution was prepared by adding 20 μL of EGDMA (cross-linker) with an additional 40 μL of Darocur 1173 into the prepolymer. The precursor solution was then spun onto a silicon wafer or glass slide or cast in a cylindrical PDMS mold, followed by UV exposure immediately. For PCC hybrid gels, PCC particles were added into the hydrogel precursor solution, with a wide range of PCC volume fraction, from 0.02 to 0.20 (weight fraction: 0.05−0.40) (see Table S3 in the Supporting Information). To improve the dispersion of PCC particles in the hydrogel, the mixture was sonicated for at least 1 h at 25 °C, followed by UV curing.

Characterization. The viscosities of the prepolymer and precursor solutions were measured by a Gemini advanced rheometer (Gemini 150, Bohlin Instruments) using a Pettier heating system (Bohlin Instruments) with a cone and plate geometry (40 mm, 2°) at 25 °C. The linear shear viscosity was measured by applying a shear ramp from 0.01 to 100 Pa. To study the interaction between the filler particles and the polymer matrix, FT-IR spectra were collected on Nexus 470 FT-IR spectrometer (Nicolet) from the neat and hybrid hydrogel precursors spin-coated on Si wafers, followed by photo-cross-link. The PCC particles dispersed in methanol were also spin-coated onto a silicon wafer as control. X-ray diffraction measurements employed a Bruker-Nonius FR591 fine-focus generator with a Cu target (λ = 1.542 Å), mirror−monochromator optics, and a Bruker HiStar wire detector. Measurements were carried out at fixed sample−detector distances of 124 cm for small-angle X-ray scattering (SAXS) and 11 cm for wide-angle X-ray scattering (WAXS) measurements. The scattered intensity was recorded for the scattering vectors, $q = 4\pi \sin(\theta)/\lambda$ (where 2θ is the scattering angle) in the range $0.02\ \text{Å}^{-1} \le q \le 0.17\ \text{Å}^{-1}$ for the SAXS and $0.2\ \text{Å}^{-1} \le q \le 1.7\ \text{Å}^{-1}$ for the WAXS measurement, respectively. Primary data analysis was performed using Datasqueeze.[34] To study the dispersion of the particles, scanning electron microscopy (SEM) images were obtained on FEI Strata DB235 focused ion beam with an acceleration voltage of 5 kV. Since the water uptake in the hybrid gels was small, no significant change in PCC particle distribution was observed from samples freeze-dried vs those dried in air. For SEM images, all the samples were dried in air.

Swelling Measurements. Cylindrical gels (6.5 mm in radius and 0.6−0.8 mm in thickness) were cured in PDMS molds, peeled off, and immersed in distilled water for at least 3 days to equilibrate the swelling. Equilibrium water weight fraction of the hydrogels, $\phi_w = (W_e - W_{dry})/W_{dry}$, was calculated by measuring the film weight in dry state (W_{dry}) and in swollen state (W_e). The extractable monomer fraction of the hydrogels, $\phi_{em} = (W_i - W_{dry})/W_i$, was calculated from the initial weight of the cross-linked gel (W_i) and the weight of the gel dried after swollen to equilibrium (W_{dry}).

Mechanical Testing. Frequency-dependent shear modulus of the equilibrated swollen cylindrical hydrogels (see above for preparation) at 25 °C were measured by using a Gemini advanced rheometer (Gemini 150, Bohlin Instruments) with a Pettier heating system (Bohlin Instruments) with parallel plate geometry. Diameter and thickness of the gels were measured precisely prior to each experiment (typically 6−6.5 mm in radius and 0.6−0.8 mm in thickness). Compression experiments were performed on an Instron test machine (Model 4206) using a 1 kN load cell. In a typical experiment, stainless steel punch was brought into contact with the hydrogel at a constant crosshead speed of 0.4 mm/s, and it was immediately retracted when a maximum compressive load, in the range of 0.2−0.9 kN, was reached. Load and displacement data were collected during the experiment. Stress relaxation experiments were performed by keeping the strain constant over a period of time, typically 1000 s, after the maximum compressive load was reached. The change in the compressive load was recorded over time under constant strain.

Results and Discussion

PCC hybrid hydrogels and neat hydrogels (both bulk and thin films) were prepared from photo-cross-linkable precursor solution as illustrated in Figure 1a. The bulk gels (typically 0.6−0.8 mm thick) were fabricated by using a cylindrical PDMS mold, where the precursor solution was poured in and exposed to UV light. Thin film gels (thickness of 20−200 μm) were obtained by spin-coating the precursor solutions on to a glass slide or silicon wafer, followed by UV exposure. As seen in Figure 1b, when the loading of PCC particles (aragonite, AR = 4.2) was increased, the film changed from transparent to increasingly white due to the random scattering of PCC particles and air voids between them. Here we note that the composition of the hydrogels, thus, precursor viscosity, could greatly affect the maximum loading of PCC particles, whereas the particle size and aspect ratio will determine the network percolation threshold, which in turn influence the hybrid gel's mechanical properties. Such effects diminish when exceeding the threshold. Since our hydrogel system consisted of water-soluble PHEMA and glassy, water-insoluble PMMA, by varying the HEMA to MMA ratio, we fine-tuned the structural and mechanical properties of the (hybrid) hydrogels. PCC loading in this study was controlled below the percolation threshold to investigate the effect of particle size and aspect ratio. First, we studied the effect of HEMA/MMA composition to swelling and mechanical properties of the neat hydrogels.

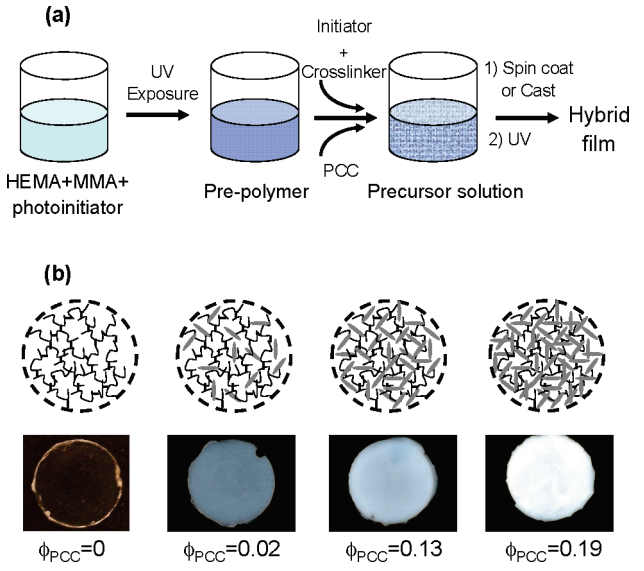

Figure 1. (a) Schematic illustration showing the fabrication of nanocomposite hydrogels. (b) Schematic structures and optical images of cross-linked PHEMA-*co*-PMMA gels loaded with aragonite PCC particles (AR = 4.2). PCC particle concentration is indicated in each image.

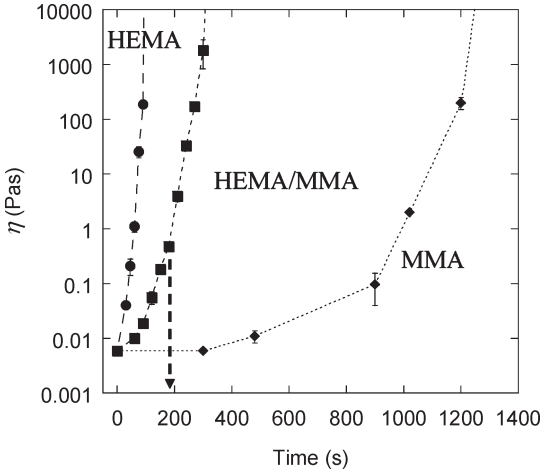

Figure 2. Effect of UV exposure time (t_{UV}) on viscosities of HEMA, HEMA:MMA (60:40 wt %), and MMA prepolymers. The arrow indicates the viscosity of HEMA:MAA prepolymer used in our experiments.

PHEMA-*co*-PMMA Hydrogels. The preparation of viscous prepolymer solution was critical to the gelation process and control of the PCC dispersion in the gel, which in turn played an important role in the physical properties of the hybrid hydrogels. Previously, we have shown that oxygen dissolved in the mold could inhibit the free-radical polymerization of the monomers and later cross-linking of the precursor solution, even if the cross-linking was carried out under nitrogen.[33] Moreover, monomers could diffuse into the PDMS mold, causing swelling and deformation of the mold. By partially copolymerizing the HEMA and MMA or other monomers, we successfully replica molded dense (up to 4.4×10^7 pillars/cm^2), high-aspect-ratio (up to 12) hydrogel pillar arrays with feature size ranging from 350 nm to 1 μm through a two-stage process.[33] To understand the kinetics of polymerization, thus, offering a tool to optimize the viscosity of the prepolymers, we measured the average linear shear viscosities of prepolymers of PHEMA, PMMA, and PHEMA-*co*-PMMA (60/40 wt %) as a function of UV exposure time (see Figure 2). Compared to PHEMA prepolymers,

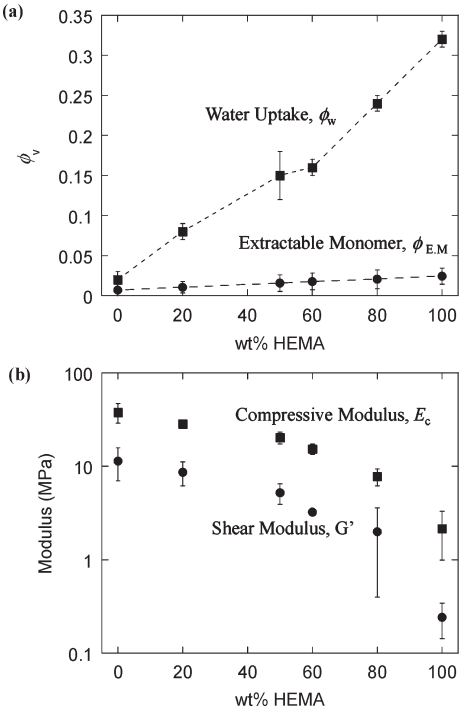

Figure 3. (a) Equilibrium water fraction, ϕ_W, and extractable monomer fraction, ϕ_{EM}, vs HEMA composition in the PHEMA-*co*-PMMA hydrogels. (b) Dependence of storage modulus, G', and compressive modulus, E_c, on HEMA composition. Hydrogels were equilibrated in distilled water for 3 days.

from which we observed a significant increase in the viscosity within a short UV exposure time ($t_{uv} = 50-90$ s), much longer exposure time ($t_{uv} = 1000-1200$ s) was needed to reach the same viscosity when polymerizing MMA monomers. The viscosity of PHEMA-*co*-PMMA prepolymers increased in a similar trend as that of PHEMA; however, an induction period was obvious at the beginning of the reaction, which indicated that the initial polymerization of the HEMA/MMA mixture was hindered by the slow polymerization rate of MMA monomers. For 60/40 wt % HEMA-*co*-MMA prepolymer, $\eta = 1.6 \pm 0.8$ Pa s ($t_{uv} = 180-200$ s) was chosen as an optimum viscosity for our experiments, which was low enough to provide good flow properties for later PCC dispersion yet high enough to limit oxygen diffusion to warrant uniform curing of the hybrid hydrogel throughout the film.

The PHEMA-*co*-PMMA prepolymer was photo-cross-linked with EGDMA, which were then equilibrated in water to investigate the water absorption, in comparison to that of the hybrid hydrogels (see Table S2 in the Supporting Information). To control the water uptake in the hydrogels, we varied the composition of water-soluble HEMA to glassy, hydrophobic MMA in the initial monomer mixture. For neat PMMA gels, equilibrium water fraction is $\phi_w = 0.03$, in comparison to $\phi_w = 0.33$ for neat PHEMA gels, a 10-fold increase. A gradual increase of ϕ_w was observed with the increase of HEMA concentration in the PHEMA-*co*-PMMA gels (Figure 3a). It should be noted that uncured monomers/oligomers could leach out during swelling, thus changing both the structural and mechanical properties of the hydrogels as well as complicating the biocompatibility. As seen in Figure 3a, the extractable monomer fraction (ϕ_{em}) in the PHEMA-*co*-PMMA hydrogels was almost insignificant at all compositions in our system, further supporting the advantage of the two-stage polymerization process.

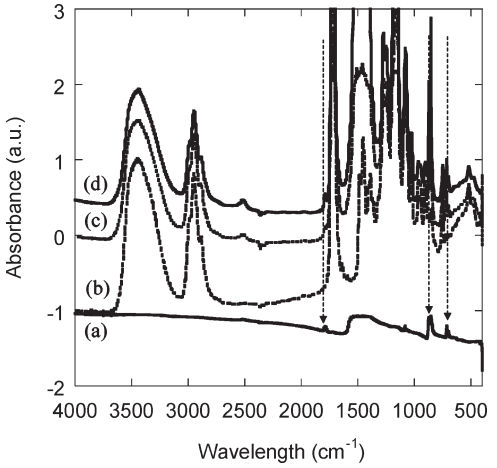

Figure 4. FT-IR spectra of (a) aragonite PCC (AR = 6.6), (b) cross-linked PHEMA-*co*-PMMA and nanocomposite gels loaded with aragonite PCC (AR = 6.6) with $\phi_{PCC} = 0.08$ (c) and $\phi_{PCC} = 0.19$ (d). Arrows with dashed lines indicate the three distinct peaks, 1799−1781, 715−703, and 875−856 cm^{-1}, of aragonite calcium carbonate.

In study of the mechanical behavior of the swollen hydrogels, we observed that the shear moduli, G, decreased by more than 40-fold, from 11 MPa (neat PMMA) to 0.25 MPa (neat PHEMA), as the HEMA composition increased in the PHEMA-*co*-PMMA hydrogels (Figure 3b), which was consistent with the study of equilibrium water fraction. When MMA composition was increased, the film became dehydrated and brittle. In the following experiments, we chose the HEMA to MMA ratio as 60 to 40 wt % ($\phi_w \sim 0.18$ and $G \sim 3$ MPa) as a model system to prepare the hybrid gels.

PHEMA-*co*-PMMA/PCC Hybrid Hydrogels. To study the effect of filler morphology, size, and aspect ratio (AR) on structural and mechanical properties of the hybrid hydrogels, we mixed needle-shape aragonite PCC (particle size of 380−1250 nm and AR of 4.2−6.6) and rhombic calcite PCC (particle size of 50−150 nm and AR of ∼1) with prepolymer solutions, with particle volume fraction in the hydrogels ranging between 0.02 and 0.20 (see Table S3 in the Supporting Information). In nanocomposites the filler particles can interact with the network framework through covalent or hydrogen bonding or simply by physical mixing into the network structure, which in turn influence the mechanical properties of the hybrid system. In addition, the distribution or packing of the fillers, i.e., whether they are randomly distributed, aligned, or highly ordered in the network, could affect the network percolation threshold and anisotropy. Therefore, it is critical to control the structure of the hybrid gels, i.e., particle dispersion and particle−polymer interactions.

Using FT-IR, we first investigated the nature of the interaction between PCC particles and hydrogel network. As seen in Figure 4, three distinct peaks attributed to calcium carbonate, 1799−1781, 715−703, and 875−856 cm^{-1} (Figure 4a), were clearly identified in the spectra of hybrid hydrogels (Figure 4c,d), and the peak intensity increased with the PCC loading. The neat PMMA-*co*-PHEMA hydrogel (Figure 4b) showed four characteristic bands: 2937 cm^{-1} (aliphatic C−H stretching), 1732 cm^{-1} (C═O stretching), and 1194 and 1147 cm^{-1} (C−O stretching). The shift of these bands in a composite can be an indication of covalent bonding or specific interaction, such as hydrogen bonding, between the filler and matrix material. However, we did not observe any shift of these bands nor additional peaks in the PCC hybrid gels, which suggested that the PCC particles were simply physically mixed in the gel network.

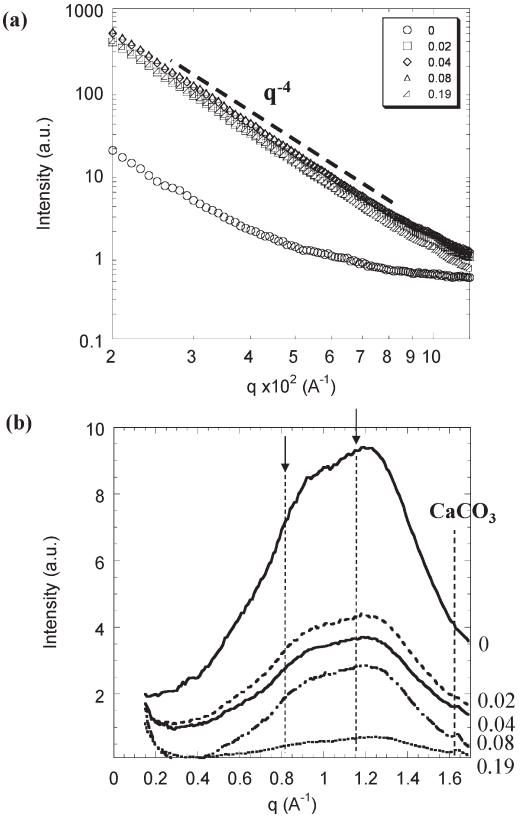

Figure 5. Scattering intensity obtained from (a) small-angle X-ray scattering (SAXS) and (b) wide-angle X-ray scattering (WAXS) spectra of aragonite PCC (AR = 6.6)/PHEMA-*co*-PMMA hybrid gels. Number in the legend represents PCC particle volume fraction (ϕ_{PCC}).

To confirm this, both small-angle X-ray scattering (SAXS) and wide-angle X-ray scattering (WAXS) were performed to study the structures of the hybrid gels at room temperature. For dry PHEMA-*co*-PMMA/PCC hybrid gels with aragonite PCC particles (particle size 1.25 μm, AR = 6.6) and volume fraction from 0.02 to 0.19 (Figure 5a), a Porod-type scattering ($I \propto q^{-4}$) in SAXS was observed, indicating random distribution of PCC particles within the gel. Supporting this, in the WAXS patterns, neat PHEMA-*co*-PMMA hydrogel showed a broad diffuse peak at $q = 0.9-1.3$ Å^{-1} (Figure 5b), indicating a short-range ordering in the cross-linked network with an average polymer chain to chain nearest-neighbor distance of $2\pi/q = 5-7$ Å^{-1}. In contrast, a well-defined feature at $q = 1.65$ Å^{-1} appeared in aragonite PCC hybrid gels, corresponding to $d_{200} \approx 3.81$ Å^{-1} for an aragonite crystal (orthorhombic, lattice parameters a = 7.969, b = 5.743 Å, c = 4.962 Å). The relative intensity of this aragonite diffraction peak increased significantly with the increase of PCC volume fraction. Cross-sectional SEM images of the dried gels showed that aragonite PCC particles (ϕ_{PCC} = 0.02, 0.08, and 0.19) were well dispersed but randomly distributed in the gel matrix (see Figure 6). Therefore, we expect the swelling and mechanical properties of our hybrid hydrogels should be isotropic in all directions, which is different from the case, where for example, CNTs were aligned in the polymer matrix under shearing.[27]

To investigate the equilibrium swelling properties, the PCC hybrid gels were equilibrated in DI water for at least 3 days in the same way as the swelling of PHEMA-*co*-PMMA gels. As seen in Figure 7a, the neat PHEMA-*co*-PMMA hydrogel has an equilibrium water fraction ϕ_w = 0.17 ± 0.02, and a slight decrease in the equilibrium water

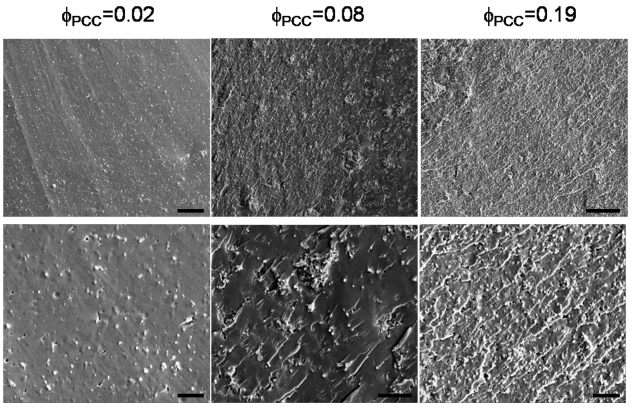

Figure 6. SEM images of hybrid gels loaded with aragonite PCC particles (AR = 5.6). Scale bars are 20 μm (top panels) and 5 μm (bottom panels). Gels were dried in air after they were swollen to equilibrium in distilled water.

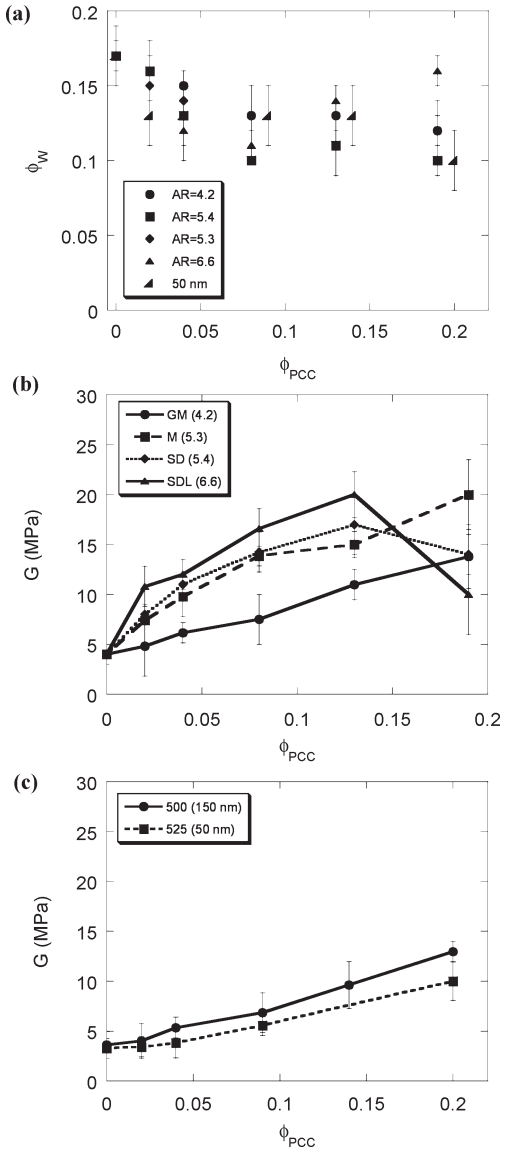

Figure 7. (a) Equilibrium water fraction, ϕ_W, of hybrid hydrogels vs PCC loading. Hydrogels were equilibrated in distilled water for at least 3 days. Labels show the PCC particles with descending aspect ratio (see Table S1). (b, c) Shear modulus of the hybrid hydrogels loaded with (b) aragonite and (c) calcite PCC particles.

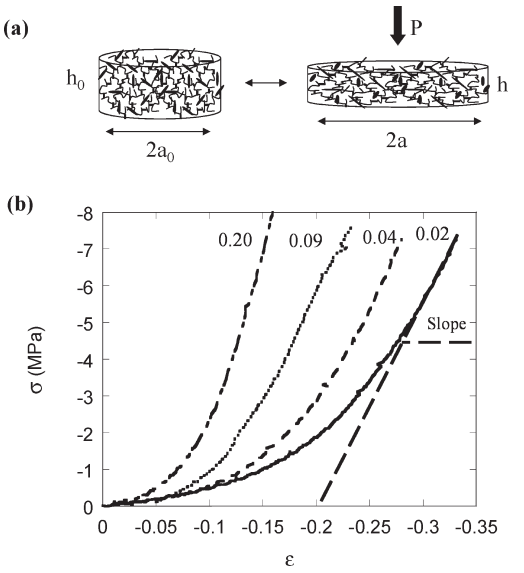

Figure 8. (a) Schematics of the sample during compression experiments. (b) Compressive stress/strain curves for hybrid hydrogels loaded with calcite PCC. The slope of each curve is used to calculate the Young's modulus of the gels.

fraction ($\phi_w \approx 0.10-0.15$) for the hybrid hydrogels was observed. Water uptake decreased with increasing PCC particle size and aspect ratio when $\phi_{PCC} < 0.08$ and became leveled off when $\phi_{PCC} > 0.08$. This may be explained by (1) decreased chain mobility upon loading of PCC particles, which will be discussed later, thus affecting water diffusion and swelling in the network, and (2) percolation of PCC in the hydrogels. As PCC particle size and aspect ratio increase, the percolation threshold of PCC in the hydrogel is lowered. Therefore, a clear decrease of the equilibrium water fraction was observed as the PCC loading was increased initially. When approaching to the PCC percolation threshold, the water uptake leveled off and became independent of the particle size and aspect ratio.

We note that hybrid hydrogel from aragonite PCC (AR = 6.6) with $\phi_{PCC} = 0.19$ had a significantly higher water fraction, which can be attributed to the increasing opaqueness of the hybrid gels with increase of particle concentration (see Figure 1) and aspect ratio. When PCC volume fraction was greater than 0.2, it became increasingly difficult to disperse PCC particles in the hydrogel precursors.

The mechanical properties of the hybrid hydrogels under both low and high strains were characterized by combination of parallel plate shear rheology and uniaxial compression tests. The swollen hybrid hydrogels behave as elastic solids, with $G' \gg G''$ and very little frequency dependence of the moduli within 0.1−100 Hz. The measured moduli are in the range of 7−20 MPa (Figure 7b) for the aragonite PCC hybrid hydrogel. The shear moduli increased when increasing the particle size, concentration, and aspect ratio. The highest increase, 4-fold, was observed for the largest particle size (1.25 μm) and AR (6.6) at the lowest volume fraction of PCC, $\phi_{PCC} = 0.12$. A 4-fold increase of modulus was achieved for medium sized particles (0.8 μm) and AR (5.3) at a higher loading, $\phi_{PCC} = 0.19$. For the smallest particle (0.38 μm) and AR (4.2), a maximum of 3-fold increase was observed for $\phi_{PCC} = 0.19$. Consistent with the swelling results, this trend did not hold for PCC with AR = 6.6 and $\phi_{PCC} = 0.19$, which we attributed to the decreased cross-linking density due to increased opacity of the films at higher PCC loading (see earlier discussion). For aragonite PCC (AR = 6.6), only a viscous

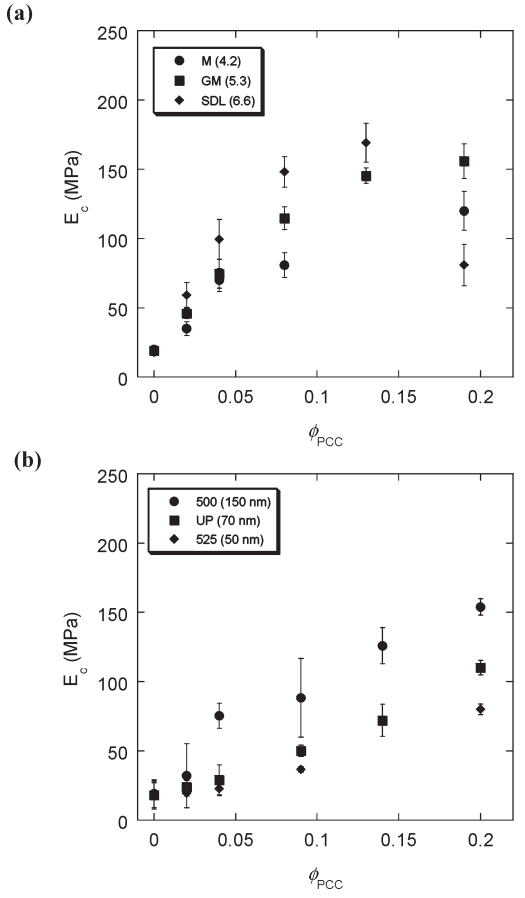

Figure 9. Compressive modulus (E_c) vs PCC volume fraction for nanocomposite hydrogels loaded with (a) aragonite and (b) calcite PCC particles. The labels denote aspect ratio for (a) and particle size for (b).

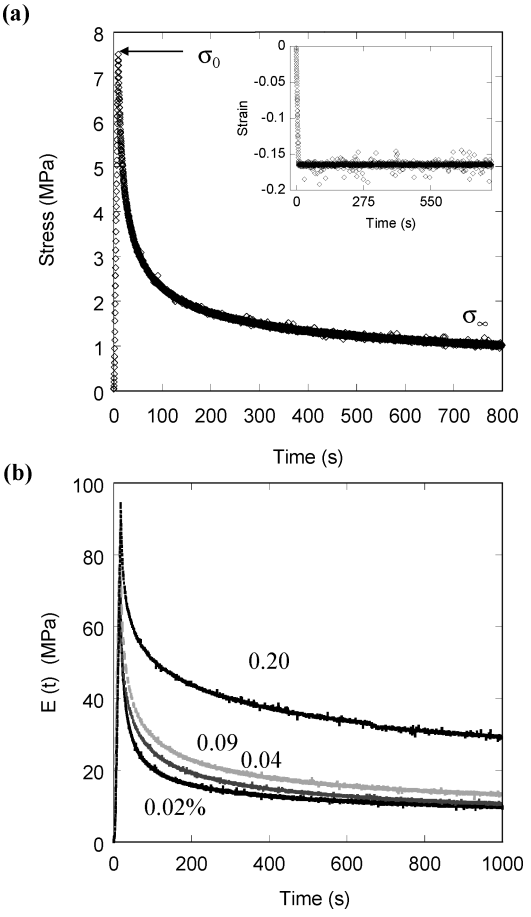

Figure 10. (a) A typical stress relaxation curve of aragonite PCC (AR = 4.2, ϕ_{PCC} = 0.04) hybrid gels over time. The solid curve in the stress plot is a generalized Maxwell model fit to the experimental data. (b) Stress relaxation modulus of aragonite PCC hybrid gels (AR = 4.2) vs time at different PCC loadings. Number in the legend represents PCC volume fraction (ϕ_{PCC}).

liquid was obtained for $\phi_{PCC} > 0.2$ after UV exposure for extended time. Compared to aragonite PCC hybrid gels, the shear moduli of calcite PCC hybrid gels (particle size of 50−170 nm) were significantly lower, in the range of 4−13 MPa (see Figure 7c), supporting the importance of particle size and aspect ratio to the mechanical properties.

Further, we conducted uniaxial compression and stress relaxation experiments on hybrid gels. In a typical uniaxial compression experiment, cylindrical gel with an initial diameter of $2a_0$ and an initial height of h_0 was compressed at a constant speed to a maximum load of 8 MPa (Figure 8a), followed by immediate retraction to 0.01 MPa. After 5 min, the next cycle of compression was applied. Figure 8b shows a typical nominal stress/strain plot for the hybrid hydrogels for increasing particle concentration. Compressive stress is defined as

$$\sigma = P/(\pi a_0^2) \quad (1)$$

where P is the load. The strain is $\varepsilon = E_c(\lambda - \lambda^{-2})$, where the deformation parameter $\lambda = h/h_0$ ($\lambda_z = l$ and $\lambda_x = \lambda_y = \lambda^{-1/2}$) and h is the instantaneous height of the gel. The stress−strain relationship for hybrid hydrogels is shown in Figure 8, from which the compressive modulus (Young's modulus, E_c) can be calculated:

$$\sigma = E_c(\lambda - \lambda^{-2}) \quad (2)$$

The compressive moduli are in the range of 40−180 MPa for aragonite PCC and 20−150 for calcite PCC. We observed a similar trend in E_c with increasing PCC volume fraction (ϕ_{PCC}) for hybrid hydrogels from both aragonite and calcite PCC. However, E_c was significantly higher from aragonite PCC than that of calcite PCC, especially at the lower particle volume fraction. This result is consistent with the observation of shear modulus of hybrid hydrogels from different PCC's, where the increase of modulus can be attributed to larger particle size and higher aspect ratio of the aragonite particles. For aragonite particles at the same particle volume fraction E_c increased with increasing aspect ratio, whereas for calcite PCC's, close to spherical morphology with AR ≈ 1, higher modulus were obtained from hydrogels with larger particles.

In compression tests, we performed five consecutive loading cycles with a waiting time of 1−2 min between each cycle. There was an increase in the compressive modulus between the first and second loading, which remained stable afterward. The modulus was recovered when the hybrid hydrogels were rested for at least 1 h after each loading cycles. This behavior resembles the so-called "Mullins effect" observed for filled rubbers, where longer relaxation time is needed for the system to recover from the prior loading.[8] To confirm this, we performed stress relaxation experiments under a constant strain, which would also provide valuable information about chain mobility and, thus, the effect of filler morphology, size, and aspect ratio on network.

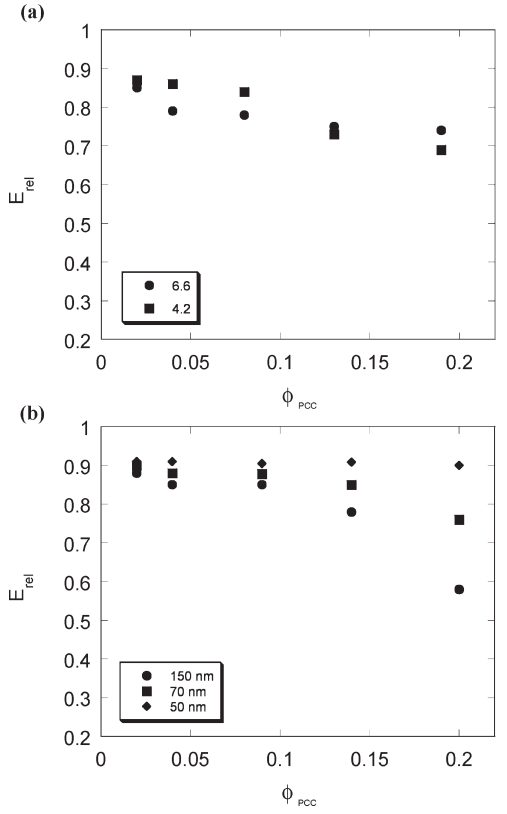

Figure 11. Relative stress relaxation modulus, E_{rel}, for hybrid hydrogels loaded with (a) aragonite PCC and (b) calcite PCC particles.

In a typical stress relaxation experiment, the cylindrical hydrogel was compressed to a maximum load of 8 MPa, which was immediately released for the first two cycles. The gel was kept under constant strain, ε_0, and waited for $t \sim 1000$ s after the third loading. The initial stress, σ_0, obtained during maximum loading relaxed over time and reached a plateau value at σ_∞ ($t = 1000$ s), as shown in Figure 10a (for aragonite PCC, AR = 4.2, and $\phi_{PCC} = 0.04$). In a stress relaxation experiment, time-dependent stress, $\sigma(t)$, can be expressed by a generalized Maxwell model:

$$\sigma(t) = \varepsilon_0[\sum_{j=1}^{n} E_j e^{-t/\tau_j}] + \varepsilon_0 E_\infty \quad (3)$$

where τ is the relaxation time, E is the relaxation modulus, and E_∞ is the plateau modulus. E at $t = 1000$ s is defined as the plateau modulus for our experiments. The time-dependent modulus can be represented by

$$E(t) = [\sum_{j=1}^{n} E_j e^{-t/\tau_j}] + E_\infty \quad (4)$$

As seen in Figure 10b, for hybrid hydrogels loaded with aragonite PCC particles (AR = 4.2) the relaxation curve shifts upward with increasing particle concentration, indicating an increase in plateau modulus (E_∞). This can be explained by the decreased free volume in the hydrogel network when increasing PCC loading, leading to an enhanced particle−polymer interactions. Using a third-order polynomial fitting to Figure 10, we obtained the relaxation time as $\tau_1 = 5-7$ s, $\tau_2 = 35-40$ s, and $\tau_3 = 330-490$ s (for $\varepsilon_0 = 0.2-0.5$). The corresponding relative relaxation modulus, $E_{rel} = (E_0 - E_\infty)/E_0$, is shown in Figure 11. For hybrid hydrogels from calcite PCC E_{rel} was the highest for the smallest PCC particles, 50 nm, and independent of particle volume fraction. For 70 and 150 nm calcite particles, E_{rel} decreased significantly when $\phi_{PCC} > 0.15$, and the 150 nm ones showed the largest drop. In the aragonite hybrid hydrogel systems, both PCC particles, AR = 4.2 and 6.6, showed similar trend of E_{rel} decreased with PCC loading. These results suggest that the network mobility is decreased when increasing the loading of PCC particles, which restricts the motion of polymer chains. At the same time, when compressed (see Figure 8a), the PCC particles are brought closer to each other, approaching the percolation threshold. Therefore, it becomes increasingly more difficult for particles to rotate or slide with the increased particle aspect ratio and size. When the particle size is small and more or less spherical, such as in the case of 50 nm calcite PCC, the system is far away from percolation threshold and relaxes efficiently without impacted by the particle concentration.

Conclusions

We prepared PHEMA-*co*-PMMA (hybrid) hydrogels by a two-stage process, including partial photopolymerization of the monomer mixture to form a HEMA-*co*-MMA prepolymer, followed by photo-cross-linking of the precursor solution dispersed with PCC particles. By varying the composition of hydrophilic HEMA vs glassy MMA, we can fine-tune the polymerization kinetics, viscosity of the prepolymer, water swellability, and structural and mechanical properties of the hydrogel network. For neat PMMA gels the equilibrium water fraction $\phi_w = 0.03$ was obtained with shear modulus $G = 11$ MPa, and Young's modulus $E_c = 38$ MPa, whereas for neat PHEMA gels a 10-fold increase of $\phi_w = 0.33$ was observed, resulting in much weaker gels with $G = 0.24$ MPa and $E_c = 3$ MPa.

We used PHEMA-*co*-PMMA hydrogels composed of 60 wt % HEMA and 40 wt % MMA with $\phi_w \sim 0.18$, $G = 2$ MPa, and $E_c = 18$ MPa as a model system for preparation of the hybrid gels. FT-IR suggested that the PCC particles were physically mixed with the polymers to support the hydrogel network. SAXS, WAXS, and SEM images further revealed that particles were randomly dispersed in the gel network, leading to isotropic mechanical behaviors. Compared to the neat hydrogels, the water swellability of hybrid gels was slightly decreased, which, however, showed no significant dependency on particle properties. A significant increase in both shear and compressive moduli were observed in hybrid hydrogels, favoring larger particle size and aspect ratio. The highest values were obtained from aragonite PCC with AR = 6.6, a 4-fold increase in shear modulus, and a 10-fold increase in compressive modulus. Consistent with modulus data network mobility decreased with increasing particle concentration, particle size, and aspect ratio, and hybrid gels from calcite PCC showed more efficient stress relaxation in comparison to that from aragonite PCC particles.

Although we focused on PHEMA-*co*-PMMA hydrogels here, we believe our two-stage gel preparation method could be conveniently applied to many other photo-cross-linkable polymer systems. More importantly, the study of structural and mechanical properties of the hybrid gels as a function of PCC particle size, morphology, aspect ratio, and loading offers us new insights to manipulate the hybrid gels for a wide range of potential applications, including coatings, cosmetics, and substrates or scaffolds for tissue engineering.

Acknowledgment. This research is supported in part by Johnson and Johnson Consumer and Personal Products Worldwide, a division of Johnson & Johnson Consumer Companies,

Inc. (JJCPPW), and NSF/MRSEC (DMR05-20020). We are grateful to Dinesh Chandra on discussion of the formulation of hydrogels, Dr. A. Radin for helping the mechanical testing, and Andre Soshinski and Dr. Robert Gambogi (JJCPPW) for helpful discussions.

Supporting Information Available: Properties of PCC particles; equilibrium water volume fraction (ϕ_w), extractable monomer volume fraction ($\phi_{e.m}$), shear modulus (G), and compressive modulus (E_c) of various PHEMA-*co*-PMMA hydrogels; weight fraction (ϕ_w) and volume fraction (ϕ_{PCC}) of the PCC particles in PHEMA-*co*-PMMA hybrid hydrogels. This material is available free of charge via the Internet at http://pubs.acs.org.

References and Notes

(1) Mano, J. F. *Adv. Eng. Mater.* **2008**, *10*, 515.
(2) Nicodemus, G. D.; Bryant, S. J. *Tissue Eng. B* **2008**, *14*, 149.
(3) Park, Y. D.; Tirelli, N.; Hubbell, J. A. *Biomaterials* **2003**, *24*, 893.
(4) Guvendiren, M.; Messersmith, P. B.; Shull, K. R. *Biomacromolecules* **2008**, *9*, 122.
(5) Gong, J. P.; Katsuyama, Y.; Kurokawa, T.; Osada, Y. *Adv. Mater.* **2003**, *15*, 1155.
(6) Tanaka, Y.; Kuwabara, R.; Na, Y. H.; Kurokawa, T.; Gong, J. P.; Osada, Y. *J. Phys. Chem. B* **2005**, *109*, 11559.
(7) Tsukeshiba, H.; Huang, M.; Na, Y. H.; Kurokawa, T.; Kuwabara, R.; Tanaka, Y.; Furukawa, H.; Osada, Y.; Gong, J. P. *J. Phys. Chem. B* **2005**, *109*, 16304.
(8) Webber, R. E.; Creton, C.; Brown, H. R.; Gong, J. P. *Macromolecules* **2007**, *40*, 2919.
(9) Gutowska, A.; Bae, Y. H.; Jacobs, H.; Feijen, J.; Kim, S. W. *Macromolecules* **1994**, *27*, 4167.
(10) Zaroslov, Y. D.; Philippova, O. E.; Khokhlov, A. R. *Macromolecules* **1999**, *32*, 1508.
(11) Zhang, J.; Peppas, N. A. *Macromolecules* **2000**, *33*, 102.
(12) Djonlagic, J.; Petrovic, Z. S. *J. Polym. Sci., Part B* **2004**, *42*, 3987.
(13) Muniz, E. C.; Geuskens, G. *Macromolecules* **2001**, *34*, 4480.
(14) Webber, R. E.; Shull, K. R. *Macromolecules* **2004**, *37*, 6153.
(15) Kong, H. J.; Wong, E.; Mooney, D. J. *Macromolecules* **2003**, *36*, 4582.
(16) Donati, I.; Holtan, S.; Morch Yrr, A.; Borgogna, M.; Dentini, M.; Skjak-Braek, G. *Biomacromolecules* **2005**, *6*, 1031.
(17) Haraguchi, K.; Li, H. J. *Macromolecules* **2006**, *39*, 1898.
(18) Haraguchi, K.; Takehisa, T.; Fan, S. *Macromolecules* **2002**, *35*, 10162.
(19) Miyazaki, S.; Endo, H.; Karino, T.; Haraguchi, K.; Shibayama, M. *Macromolecules* **2007**, *40*, 4287.
(20) Durmus, A.; Kasgoz, A.; Macosko, C. W. *J. Macromol. Sci., Part B* **2008**, *47*, 608.
(21) Nie, J. J.; Du, B. Y.; Oppermann, W. *Macromolecules* **2005**, *38*, 5729.
(22) Paul, D. R.; Robeson, L. M. *Polymer* **2008**, *49*, 3187.
(23) Xiang, Y. Q.; Chen, D. J. *Eur. Polym. J.* **2007**, *43*, 4178.
(24) Kim, H.; Macosko, C. W. *Macromolecules* **2008**, *41*, 3317.
(25) Haggenmueller, R.; Gommans, H. H.; Rinzler, A. G.; Fischer, J. E.; Winey, K. I. *Chem. Phys. Lett.* **2000**, *330*, 219.
(26) Winey, K. I.; Vaia, R. A. *MRS Bull.* **2007**, *32*, 314.
(27) White, S. I.; DiDonna, B. A.; Mu, M. F.; Lubensky, T. C.; Winey, K. I. *Phys. Rev. B* **2009**, *79*, 024301.
(28) Meldrum, F. C. *Int. Mater. Rev.* **2003**, *48*, 187.
(29) Manroshan, S.; Baharin, A. *J. Appl. Polym. Sci.* **2005**, *96*, 1550.
(30) Pickles, M. J.; Evans, M.; Philpotts, C. J.; Joiner, A.; Lynch, R. J. M.; Noel, N.; Laucello, M. *Int. Dent. J.* **2005**, *55*, 197.
(31) Liimtainen, H.; Kokko, S.; Rousu, P.; Niinimaki, J. *Tappi J.* **2006**, *5*, 11.
(32) Solah, V. A.; Staines, V.; Honda, S.; Limley, H. A. *J. Food Sci.* **2007**, *72*, S560.
(33) Chandra, D.; Taylor, J. A.; Yang, S. *Soft Matter* **2008**, *4*, 979.
(34) http://www.datasqueezesoftware.com.